

Search for the decay $B^0 \rightarrow DK^{*0}$ followed by $D \rightarrow K^-\pi^+$

K. Negishi,⁴⁹ Y. Horii,²⁸ Y. Onuki,⁵⁰ T. Sanuki,⁴⁹ H. Yamamoto,⁴⁹ I. Adachi,⁹ H. Aihara,⁵⁰ D. M. Asner,³⁷ T. Aushev,¹⁵ A. M. Bakich,⁴⁴ Y. Ban,³⁸ K. Belous,¹⁴ B. Bhuyan,¹⁰ A. Bondar,² T. E. Browder,⁸ M.-C. Chang,⁵ A. Chen,³⁰ P. Chen,³² B. G. Cheon,⁷ K. Chilikin,¹⁵ R. Chistov,¹⁵ I.-S. Cho,⁵⁶ K. Cho,¹⁹ Y. Choi,⁴³ J. Dalseno,^{25,46} Z. Doležal,³ Z. Drásal,³ A. Drutskoy,¹⁵ S. Eidelman,² J. E. Fast,³⁷ V. Gaur,⁴⁵ N. Gabyshev,² Y. M. Goh,⁷ J. Haba,⁹ H. Hayashii,²⁹ Y. Hoshi,⁴⁸ W.-S. Hou,³² H. J. Hyun,²¹ T. Iijima,^{28,27} K. Inami,²⁷ A. Ishikawa,⁴⁹ R. Itoh,⁹ M. Iwabuchi,⁵⁶ Y. Iwasaki,⁹ T. Iwashita,²⁹ T. Julius,²⁶ J. H. Kang,⁵⁶ T. Kawasaki,³⁴ C. Kiesling,²⁵ H. J. Kim,²¹ J. B. Kim,²⁰ J. H. Kim,¹⁹ K. T. Kim,²⁰ M. J. Kim,²¹ Y. J. Kim,¹⁹ B. R. Ko,²⁰ P. Kodyš,³ S. Korpar,^{24,16} R. T. Kouzes,³⁷ P. Krokovny,² T. Kuhr,¹⁸ Y.-J. Kwon,⁵⁶ S.-H. Lee,²⁰ J. Libby,¹¹ C. Liu,⁴¹ Y. Liu,⁴ Z. Q. Liu,¹² R. Louvot,²² D. Matvienko,² S. McOnie,⁴⁴ K. Miyabayashi,²⁹ H. Miyata,³⁴ Y. Miyazaki,²⁷ D. Mohapatra,³⁷ A. Moll,^{25,46} N. Muramatsu,³⁹ E. Nakano,³⁶ M. Nakao,⁹ S. Nishida,⁹ K. Nishimura,⁸ O. Nitoh,⁵³ S. Ogawa,⁴⁷ T. Ohshima,²⁷ S. Okuno,¹⁷ G. Pakhlova,¹⁵ H. K. Park,²¹ T. K. Pedlar,²³ R. Pestotnik,¹⁶ M. Petrič,¹⁶ L. E. Piilonen,⁵⁴ M. Röhrken,¹⁸ S. Ryu,⁴² K. Sakai,⁹ Y. Sakai,⁹ O. Schneider,²² C. Schwanda,¹³ A. J. Schwartz,⁴ K. Senyo,⁵⁵ M. E. Sevier,²⁶ M. Shapkin,¹⁴ V. Shebalin,² T.-A. Shibata,⁵¹ J.-G. Shiu,³² B. Shwartz,² A. Sibidanov,⁴⁴ F. Simon,^{25,46} P. Smerkol,¹⁶ Y.-S. Sohn,⁵⁶ E. Solovieva,¹⁵ S. Stanič,³⁵ M. Starič,¹⁶ M. Sumihama,⁶ T. Sumiyoshi,⁵² S. Suzuki,⁴⁰ G. Tatishvili,³⁷ Y. Teramoto,³⁶ K. Trabelsi,⁹ M. Uchida,⁵¹ T. Uglov,¹⁵ Y. Unno,⁷ S. Uno,⁹ P. Urquijo,¹ G. Varner,⁸ K. E. Varvell,⁴⁴ V. Vorobyev,² C. H. Wang,³¹ M.-Z. Wang,³² P. Wang,¹² M. Watanabe,³⁴ Y. Watanabe,¹⁷ E. Won,²⁰ B. D. Yabsley,⁴⁴ Y. Yamashita,³³ C. C. Zhang,¹² Z. P. Zhang,⁴¹ V. Zhilich,² V. Zhulanov,² and A. Zupanc¹⁸

(The Belle Collaboration)

¹University of Bonn, Bonn

²Budker Institute of Nuclear Physics SB RAS and Novosibirsk State University, Novosibirsk 630090

³Faculty of Mathematics and Physics, Charles University, Prague

⁴University of Cincinnati, Cincinnati, Ohio 45221

⁵Department of Physics, Fu Jen Catholic University, Taipei

⁶Gifu University, Gifu

⁷Hanyang University, Seoul

⁸University of Hawaii, Honolulu, Hawaii 96822

⁹High Energy Accelerator Research Organization (KEK), Tsukuba

¹⁰Indian Institute of Technology Guwahati, Guwahati

¹¹Indian Institute of Technology Madras, Madras

¹²Institute of High Energy Physics, Chinese Academy of Sciences, Beijing

¹³Institute of High Energy Physics, Vienna

¹⁴Institute of High Energy Physics, Protvino

¹⁵Institute for Theoretical and Experimental Physics, Moscow

¹⁶J. Stefan Institute, Ljubljana

¹⁷Kanagawa University, Yokohama

¹⁸Institut für Experimentelle Kernphysik, Karlsruher Institut für Technologie, Karlsruhe

¹⁹Korea Institute of Science and Technology Information, Daejeon

²⁰Korea University, Seoul

²¹Kyungpook National University, Taegu

²²École Polytechnique Fédérale de Lausanne (EPFL), Lausanne

²³Luther College, Decorah, Iowa 52101

²⁴University of Maribor, Maribor

²⁵Max-Planck-Institut für Physik, München

²⁶University of Melbourne, School of Physics, Victoria 3010

²⁷Graduate School of Science, Nagoya University, Nagoya

²⁸Kobayashi-Maskawa Institute, Nagoya University, Nagoya

²⁹Nara Women's University, Nara

³⁰National Central University, Chung-li

³¹National United University, Miao Li

³²Department of Physics, National Taiwan University, Taipei

³³Nippon Dental University, Niigata

- ³⁴Niigata University, Niigata
³⁵University of Nova Gorica, Nova Gorica
³⁶Osaka City University, Osaka
³⁷Pacific Northwest National Laboratory, Richland, Washington 99352
³⁸Peking University, Beijing
³⁹Research Center for Electron Photon Science, Tohoku University, Sendai
⁴⁰Saga University, Saga
⁴¹University of Science and Technology of China, Hefei
⁴²Seoul National University, Seoul
⁴³Sungkyunkwan University, Suwon
⁴⁴School of Physics, University of Sydney, NSW 2006
⁴⁵Tata Institute of Fundamental Research, Mumbai
⁴⁶Excellence Cluster Universe, Technische Universität München, Garching
⁴⁷Toho University, Funabashi
⁴⁸Tohoku Gakuin University, Tagajo
⁴⁹Tohoku University, Sendai
⁵⁰Department of Physics, University of Tokyo, Tokyo
⁵¹Tokyo Institute of Technology, Tokyo
⁵²Tokyo Metropolitan University, Tokyo
⁵³Tokyo University of Agriculture and Technology, Tokyo
⁵⁴CNP, Virginia Polytechnic Institute and State University, Blacksburg, Virginia 24061
⁵⁵Yamagata University, Yamagata
⁵⁶Yonsei University, Seoul

We report a study of the decay $B^0 \rightarrow DK^+\pi^-$ followed by $D \rightarrow K^-\pi^+$, where D indicates D^0 or \bar{D}^0 . We reconstruct the $DK^+\pi^-$ state in a phase space corresponding to $DK^*(892)^0$. The CP -violating angle ϕ_3 affects its decay rate via the interference between $b \rightarrow u$ and $b \rightarrow c$ transitions. The result is obtained from a 711 fb^{-1} data sample that contains $772 \times 10^6 B\bar{B}$ pairs collected at the $\Upsilon(4S)$ resonance with the Belle detector at the KEKB asymmetric-energy e^+e^- collider. We measure the ratio $\mathcal{R}_{DK^{*0}} \equiv \Gamma(B^0 \rightarrow [K^-\pi^+]_D K^+\pi^-) / \Gamma(B^0 \rightarrow [K^+\pi^-]_D K^+\pi^-)$ to be $(4.1_{-5.0}^{+5.6+2.8}) \times 10^{-2}$, and set an upper limit of $\mathcal{R}_{DK^{*0}} < 0.16$ at the 95% confidence level.

PACS numbers: 13.25.Hw, 11.30.Er, 12.15.Hh, 14.40.Nd

Determination of the parameters of the standard model is important as a consistency check and as a way to search for new physics. In the standard model, the Cabibbo-Kobayashi-Maskawa (CKM) matrix [1] V consists of four independent weak interaction parameters for the quark sector; the three CP -violating phases ϕ_1 , ϕ_2 and ϕ_3 are defined as the angles of one particular CKM unitarity triangle with the latter defined as $\phi_3 \equiv \arg(-V_{ud}V_{ub}^*/V_{cd}V_{cb}^*)$. This phase is less accurately determined than the other two [2]. In the usual quark-phase convention where large complex phases appear only in V_{ub} and V_{td} [3], the measurement of ϕ_3 is equivalent to the extraction of the phase of V_{ub} relative to the phases of other CKM matrix elements. To date, the ϕ_3 measurement has been advanced mainly by exploiting charged B meson decays into $D^{(*)}K^+$ final states [4–12] wherein the CP sensitivity is due to the interference between the two amplitudes of $\bar{D}^{(*)0}$ and $D^{(*)0}$ decays into a common final state.

In this paper, we consider the neutral meson decay $B^0 \rightarrow DK^{*0}$ as an alternative process for measuring the angle ϕ_3 . As shown by the Feynman diagrams in Fig. 1, a weak decay of the B meson is tagged by the K^{*0} decaying into $K^+\pi^-$ [13]. We measure the ratio $\mathcal{R}_{DK^{*0}}$ [14, 15]

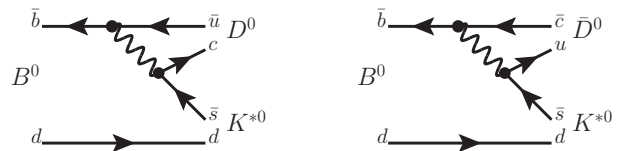


FIG. 1: Diagrams for the $B^0 \rightarrow D^0 K^{*0}$ and $B^0 \rightarrow \bar{D}^0 K^{*0}$ decays. The ϕ_3 dependence in the $b \rightarrow u$ transition is extracted from the interference of the two decay paths, which occurs when the \bar{D}^0 and D^0 mesons decay to the same final state.

defined as

$$\begin{aligned} \mathcal{R}_{DK^{*0}} &\equiv \frac{\Gamma(B^0 \rightarrow [K^-\pi^+]_D K^+\pi^-)}{\Gamma(B^0 \rightarrow [K^+\pi^-]_D K^+\pi^-)} \\ &= r_S^2 + r_D^2 + 2kr_S r_D \cos(\delta_S + \delta_D) \cos \phi_3, \end{aligned} \quad (1)$$

where $r_D \equiv |A(D^0 \rightarrow K^+\pi^-)/A(D^0 \rightarrow K^-\pi^+)|$ is the ratio for D decay amplitudes and δ_D is the strong phase difference of the two D decays appearing in this ratio. Both r_D and δ_D have been obtained experimentally [16].

The parameters r_S , δ_S and k are defined as

$$r_S^2 \equiv \frac{\Gamma(B^0 \rightarrow D^0 K^+ \pi^-)}{\Gamma(B^0 \rightarrow D^0 K^+ \pi^-)} = \frac{\int dp A_{b \rightarrow u}^2(p)}{\int dp A_{b \rightarrow c}^2(p)}, \quad (2)$$

$$k e^{i\delta_S} \equiv \frac{\int dp A_{b \rightarrow c}(p) A_{b \rightarrow u}(p) e^{i\delta(p)}}{\sqrt{\int dp A_{b \rightarrow c}^2(p) \int dp A_{b \rightarrow u}^2(p)}}, \quad (3)$$

where $A_{b \rightarrow c}(p)$ and $A_{b \rightarrow u}(p)$ are the magnitudes of the amplitudes for the $b \rightarrow c$ and $b \rightarrow u$ transitions, respectively, and $\delta(p)$ is the relative strong phase. The variable p indicates the position in the $DK^+\pi^-$ Dalitz plot. In this analysis, we calculate the integrals over a phase space of the state $DK^*(892)^0$. In the case of a two-body B decay, r_S becomes the ratio of the amplitudes for $b \rightarrow u$ and $b \rightarrow c$ and k becomes 1. The value of r_S is expected to be around 0.4, which is obtained from $|V_{ub}V_{cs}^*|/|V_{cb}V_{us}^*|$ and depends on strong interaction effects. According to a simulation study using a Dalitz model based on recent measurements [17], the value of k is around 0.95 in the phase space of interest here. One observable \mathcal{R}_{DK^*0} is not enough to extract the four unknowns ϕ_3 , r_S , k , and δ_S . However, the measurements for other D decays such as $D \rightarrow K^+K^-$ and $K_S\pi^0$ provide additional information needed to extract ϕ_3 , where the observable \mathcal{R}_{DK^*0} should be defined in the same phase space of the B^0 decay between different D decays so that the same parameters r_S , k , and δ_S can be used. The decay in the numerator of Eq. (1) is the signal mode, referred to as the ‘‘suppressed mode,’’ while the decay in the denominator is the calibration mode referred to as the ‘‘favored mode.’’

This result is based on a data sample that contains 772×10^6 $B\bar{B}$ pairs, collected with the Belle detector at the KEKB asymmetric-energy e^+e^- (3.5 on 8 GeV) collider [18] operating at the $\Upsilon(4S)$ resonance. The Belle detector is a large-solid-angle magnetic spectrometer that consists of a silicon vertex detector, a 50-layer central drift chamber (CDC), an array of aerogel threshold Cherenkov counters (ACC), a barrel-like arrangement of time-of-flight scintillation counters (TOF), and an electromagnetic calorimeter comprised of CsI(Tl) crystals located inside a superconducting solenoid coil that provides a 1.5 T magnetic field. An iron flux-return located outside of the coil is instrumented to detect K_L^0 mesons and to identify muons. The detector is described in detail elsewhere [19].

Charged kaon and pion candidates are identified using ionization loss in the CDC and information from the ACC and the TOF. The efficiency is 85–95% and the probability of misidentification is 10–20%. We reconstruct D mesons from pairs of oppositely-charged kaon and pion candidates. We require that the invariant mass is within ± 15 MeV/ c^2 ($\pm 3\sigma$) of the nominal D^0 mass. K^{*0} candidates are reconstructed from $K^+\pi^-$ pairs. We require that the invariant mass is within ± 50 MeV/ c^2 of the nominal K^{*0} mass. We combine D and K^{*0} candi-

dates to form B^0 mesons. Candidate events are identified by the energy difference $\Delta E \equiv \sum_i E_i - E_b$ and the beam-constrained mass $M_{bc} \equiv \sqrt{E_b^2 - |\sum_i \vec{p}_i|^2}$, where E_b is the beam energy and \vec{p}_i and E_i are the momenta and energies, respectively, of the B^0 meson decay products in the e^+e^- center-of-mass (CM) frame. We select events with 5.271 GeV/ $c^2 < M_{bc} < 5.287$ GeV/ c^2 and -0.1 GeV $< \Delta E < 0.3$ GeV. In the rare case where there are multiple candidates in an event, the candidate with M_{bc} closest to its nominal value is chosen.

Among other B decays, the most serious background for the suppressed mode comes from $\bar{B}^0 \rightarrow [\bar{K}^{*0}K^+]_{D^+}\pi^-$. This decay produces the same final state as the $B^0 \rightarrow DK^{*0}$ signal, and the product branching fraction is about 10 times higher than that expected for the signal. To suppress this background, we exclude candidates for which the invariant mass of the $K^-\pi^+K^+$ system is within ± 18 MeV/ c^2 ($\pm 3\sigma$) of the nominal D^+ mass. The relative loss in the signal efficiency is 0.5%.

Large combinatorial background of true D^0 and random K^+ and π^- combinations from the $e^+e^- \rightarrow c\bar{c}$ process and other $B\bar{B}$ decays is reduced if the D^0 is a decay product of $D^{*+} \rightarrow D^0\pi^+$ by using the mass difference ΔM between the $[K^-\pi^+]_{D^+}\pi^+$ and $[K^-\pi^+]_D$ systems, where a π^+ candidate is added to the latter to form the former. If $\Delta M > 0.15$ GeV/ c^2 for any additional π^+ candidate not used in the B candidate reconstruction, the event is retained. This requirement removes 24% of $c\bar{c}$ background and 14% of $B\bar{B}$ background according to Monte Carlo (MC) simulation. The relative loss in signal efficiency is 5.0%.

To discriminate the large combinatorial background dominated by the two-jet-like $e^+e^- \rightarrow q\bar{q}$ continuum process, where q indicates u, d, s or c , a multivariate analysis is performed using the following nine variables. 1) A variable obtained from the Fisher discriminants based on modified Fox-Wolfram moments [20] where the coefficients of the Fisher discriminants are optimized using the signal and $q\bar{q}$ MC samples. This variable exploits the event topology, which is spherical and jet-like for $B\bar{B}$ and $q\bar{q}$ events, respectively. 2) The angle in the CM frame between the thrust axes of the B decay and the detected remainders. For the latter, we assign the pion mass to all the charged particles and use photons with energy above 0.1 GeV. 3) The signed difference of the vertices between the B candidate and the remaining charged tracks. For the signal event, the absolute value tends to be larger because of the longer lifetime of the B meson. 4) The angle between the K candidate from the D decay and the B candidate in the rest frame of the D candidate. Its distribution is flat for signal events but peaked near the extreme values for $q\bar{q}$ background. 5) The expected flavor dilution factor described in Ref. [21]. It ranges from zero for no flavor information to unity for unambiguous flavor assignment. B candidates tend to have a larger flavor dilution factor than $q\bar{q}$ background. 6) The

angle θ between the B meson momentum direction and the beam axis in the CM frame. The B decays follow a $1 - \cos^2 \theta$ distribution, while the $q\bar{q}$ background is nearly flat in $\cos \theta$. 7) The distance of closest approach between the trajectories of the K^* and D candidates. The value is close to zero for the signal but tends to be larger for the $c\bar{c}$ background. 8) The difference between the sum of the particle charges in the D hemisphere and the sum in the opposite hemisphere, excluding those used in the reconstruction of the B meson. The average charge difference is 0 for the signal events but $\pm 4/3$ for the $c\bar{c}$ events, depending on the flavor of the B candidate. 9) The angle between the D and $\Upsilon(4S)$ directions in the rest frame of the B candidate. The cosine distribution is about flat for signal events but peaks toward +1 for $c\bar{c}$ events.

To effectively combine these nine variables, we employ the NeuroBayes neural network package [22]. The NeuroBayes output is denoted as C_{NB} with a range of $[-1, 1]$. For example, events at $C_{\text{NB}} \sim 1$ are signal-like and events at $C_{\text{NB}} \sim -1$ are $q\bar{q}$ -like. The training for the neural network optimization is performed by using the signal and the $q\bar{q}$ MC samples, each of which contains 100,000 events after the event-selection requirements. For the latter sample, we loosen the requirement on M_{bc} to $5.23 \text{ GeV}/c^2 < M_{bc} < 5.27 \text{ GeV}/c^2$ to obtain a larger number of events, since all the input parameters have little correlation with M_{bc} .

The C'_{NB} distribution peaks at $|C_{\text{NB}}| \sim 1$ and is therefore difficult to represent with a simple analytic function. However, the transformed variable

$$C'_{\text{NB}} = \ln \frac{C_{\text{NB}} - C_{\text{NB,low}}}{C_{\text{NB,high}} - C_{\text{NB}}}, \quad (4)$$

where $C_{\text{NB,low}} = -0.6$ and $C_{\text{NB,high}} = 1.0$, has a distribution that can be modelled by a Gaussian. The events with $C_{\text{NB}} < -0.6$ are rejected. The background rejection rate is 70.5%, while the signal loss is 3.9%.

The number of signal events is obtained by a two-dimensional unbinned extended maximum likelihood fit to ΔE and C'_{NB} . The fits are applied separately for favored and suppressed modes. For both modes, we categorize five common contributions. These are the DK^{*0} signal, the $\bar{D}^0 \rho^0$ background, the combinatorial $B\bar{B}$ background, the $q\bar{q}$ background, and the backgrounds that have peaks in the signal region of ΔE and C'_{NB} (“peaking background”). In the favored mode, we include two more components: $\bar{D}^0 K^+$ and $\bar{D}^0 \pi^+$. The $B^0 \rightarrow \bar{D}^0 \rho^0$ decay satisfies the selection criteria when a pion from the ρ^0 decay is misidentified as a kaon. This component also includes other decays that satisfy the selection criteria when a pion in the final state is misidentified as a kaon. The peaking background for the suppressed mode consists of $B^0 \rightarrow [K^-\pi^+\pi^-]_D - K^+$ and $B^0 \rightarrow [K^+K^-]_{D^0} \pi^+\pi^-$ while the peaking background for the favored mode consists of $B^0 \rightarrow [K^+\pi^-\pi^-]_D - K^+$. For the $B^0 \rightarrow \bar{D}^0 K^+$ and $\bar{D}^0 \pi^+$ backgrounds, a pion

candidate is added to reconstruct K^{*0} , where the latter satisfies the selection when the π^+ is misidentified as K^+ . We prepare two-dimensional probability density functions (PDFs) for each component as a product of one-dimensional PDFs on ΔE and C'_{NB} , since the correlation between ΔE and C'_{NB} is found to be small.

The ΔE PDFs for a favored mode are parameterized by a double Gaussian for signal, a double Gaussian for $\bar{D}^0 \rho^0$, an exponential function for $B\bar{B}$ background, a linear function for $q\bar{q}$ background, a Crystal Ball function for $\bar{D}^0 K^+$, and a double bifurcated Gaussian for $\bar{D}^0 \pi^+$. The means and widths of the double-Gaussian PDFs for the signal and $\bar{D}^0 \rho^0$ components are fixed from MC samples. The mean of the ΔE distribution for $\bar{D}^0 \rho^0$ is higher than that for the signal by about 70 MeV due to misidentification of a pion as a kaon. The parameters of the exponential and linear PDFs are allowed to float. The ΔE PDF for the peaking background is defined to be that of the signal, and the yield is fixed by the world-average value of the branching fraction [23]. The mean values of ΔE for $\bar{D}^0 K^+$ and $\bar{D}^0 \pi^+$ are higher than those for the signal due to one additional pion and a misidentification for the latter mode. The shape parameters of the ΔE PDFs for these components are determined from MC and their yields are fixed by the world-average value of the branching fraction.

The C'_{NB} PDF is a sum of two Gaussians for each component. The shapes for the signal and $B\bar{B}$ background are fixed from the MC samples of each decay model. The C'_{NB} PDF for $\bar{D}^0 \rho^0$ is defined by the same function as that of $B\bar{B}$ background. The C'_{NB} PDF for the peaking background is described as a weighted sum of MC-based PDFs for all the constituents. The shape for the $q\bar{q}$ background is fixed from the M_{bc} sideband data sample in data defined by $5.23 \text{ GeV}/c^2 < M_{bc} < 5.27 \text{ GeV}/c^2$. The validity of this use of the M_{bc} sideband sample, which is reasonable since all inputs for C'_{NB} have little correlation with M_{bc} , is checked using MC samples. The C'_{NB} PDF for $\bar{D}^0 K^+$ and $\bar{D}^0 \pi^+$ is the same as that of the $B\bar{B}$ background.

The results of the fits for suppressed and favored modes are shown in Fig. 2 and presented in Table I. We obtain the ratio $\mathcal{R}_{DK^{*0}}$ to be

$$\begin{aligned} \mathcal{R}_{DK^{*0}} &= \frac{N_{\text{sup}}/\epsilon_{\text{sup}}}{N_{\text{fav}}/\epsilon_{\text{fav}}} \\ &= (4.1^{+5.6+2.8}_{-5.0-1.8}) \times 10^{-2}, \end{aligned}$$

where $N_{\text{sup}} (\text{fav})$ is the signal yield for the suppressed (favored) mode, $\epsilon_{\text{sup}} (\text{fav})$ is the detection efficiency obtained from a MC study for the suppressed (favored) mode.

We list the sources of systematic uncertainties in Table II. The uncertainties of the PDF shape parameters are estimated by varying the determined parameters of the PDFs by $\pm 1\sigma$. The uncertainties due to the C'_{NB} PDFs for $\bar{D}^0 \rho^0$, combinatorial $B\bar{B}$, $\bar{D}^0 K^+$, and $\bar{D}^0 \pi^+$ are estimated by replacing their PDFs with the signal PDF. The

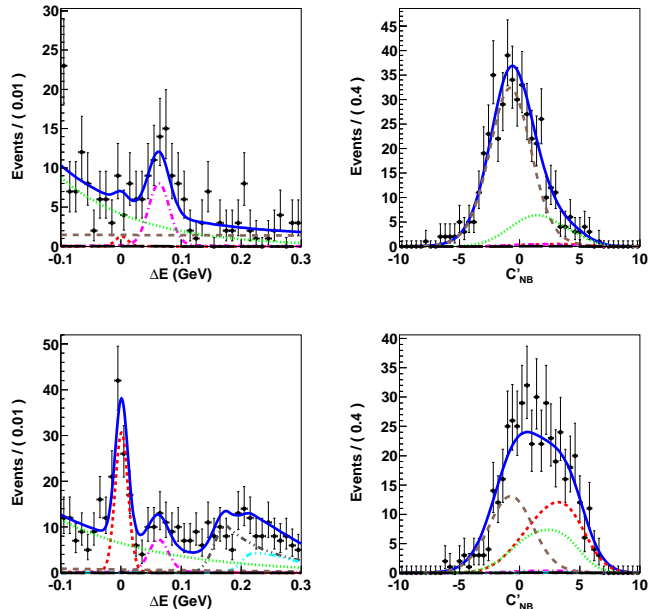


FIG. 2: The projections of the fits to data for the suppressed mode (upper) and the favored mode (lower): the ΔE projection for $3 < C'_{\text{NB}} < 10$ (left) and the C'_{NB} projection for $|\Delta E| < 0.03$ GeV (right). The fitted data samples are shown by the dots with error bars and the total PDFs are shown by the solid blue curve. Individual components are shown by the dashed red (DK^{*0} signal), the dash-dotted magenta ($\bar{D}^0\rho^0$), the short dashed green (combinatorial $B\bar{B}$ background), the long dashed brown ($q\bar{q}$ background), the very long dashed black (peaking backgrounds), the dash-dot-dotted gray (\bar{D}^0K^+), and the dash-dot-dot-dotted aqua ($\bar{D}^0\pi^+$).

uncertainty due to the PDF shape for $q\bar{q}$ is the largest systematic uncertainty. The uncertainty due to the yields of the peaking background is conservatively estimated by applying 0 and 2 times the nominal expected yields. The systematic uncertainty associated with the peaking background is small because of its small expected yield. The uncertainty due to the yields of \bar{D}^0K^+ and $\bar{D}^0\pi^+$ is estimated by taking into account the uncertainty of the efficiencies and the branching fractions. We check the fit bias by generating 10,000 pseudo-experiments for each of the suppressed and favored modes. We obtain an almost standard Gaussian distribution for the pull, and take the product of the mean of the pull and the error of the nominal fit. MC statistics and the uncertainties in the efficiencies of particle identification dominate the systematic uncertainty in detection efficiency. The uncertainties in the efficiencies of particle identifications are determined from the decay $D^{*+} \rightarrow D^0\pi^+$ followed by $D^0 \rightarrow K^-\pi^+$. The uncertainty due to the charmless $B^0 \rightarrow K^{*0}K^+\pi^-$ decay is obtained from the upper limit of its branching ratio [23] and the efficiency estimated

TABLE I: Summary of the results. The errors for N and $\mathcal{R}_{DK^{*0}}$ are statistical only.

Mode	ϵ (%)	N	$\mathcal{R}_{DK^{*0}}$
$B^0 \rightarrow [K^+\pi^-]_D K^{*0}$	21.0 ± 0.3	$190^{+22.3}_{-21.2}$	$(4.1^{+5.6}) \times 10^{-2}$
$B^0 \rightarrow [K^-\pi^+]_D K^{*0}$	20.9 ± 0.3	$7.7^{+10.6}_{-9.5}$	$(4.1^{+5.6}) \times 10^{-2}$

TABLE II: Summary of the systematic uncertainties for $\mathcal{R}_{DK^{*0}}$.

Source	Uncertainty [10^{-2}]
Signal PDFs	+0.1 – 0.2
$\bar{D}^0\rho^0$ PDFs	+0.0 – 0.1
Combinatorial $B\bar{B}$ PDFs	+1.8 – 1.2
Peaking background PDFs	+0.1 – 0.1
$q\bar{q}$ PDFs	+2.2 – 1.4
\bar{D}^0K^+ PDFs	+0.0 – 0.0
$\bar{D}^0\pi^+$ PDFs	+0.0 – 0.1
Fit bias	+0.4 – 0.0
Efficiency	+0.1 – 0.1
Charmless decay	+0.0 – 0.3
Total	+2.8 – 1.8

by assuming a non-resonant distribution in phase space. The uncertainties due to the favored mode are estimated in a similar manner as for the suppressed mode and are found to be small.

The distribution of the likelihood \mathcal{L} is obtained by convolving the likelihood in the $(\Delta E, C'_{\text{NB}})$ two-dimensional fit and an asymmetric Gaussian whose widths are the negative and positive systematic errors. We set a 95% confidence level (C.L.) upper limit for $\mathcal{R}_{DK^{*0}}$ to be $\mathcal{R}_{DK^{*0}} < 0.16$. We obtain an upper limit of $r_S < 0.4$, corresponding to 95% C.L. limit of $R_{DK^{*0}}$, by conservatively assuming that r_S is much larger than r_D so that $R_{DK^{*0}} = r_S^2$. The uncertainties due to the signal yield of the favored mode are found to be negligible.

In summary, we report a result of the measurement of the ratio $\mathcal{R}_{DK^{*0}}$, using a 711 fb^{-1} data sample collected by the Belle detector. We obtain $\mathcal{R}_{DK^{*0}} = (4.1^{+5.6+2.8}_{-5.0-1.8}) \times 10^{-2}$, which can be used to extract ϕ_3 by combining with other observables related to the same dynamical parameters r_S , δ_S and k . Since the value of $\mathcal{R}_{DK^{*0}}$ is not significant, we set an upper limit of $\mathcal{R}_{DK^{*0}} < 0.16$ (95% C.L.); this is the most stringent limit to date. Possible reasons for the small r_S are destructive interference between the two D decays, destructive interference between DK^{*0} and other $DK^+\pi^-$ states, or a small ratio of magnitudes of amplitudes for $B^0 \rightarrow D^0K^{*0}$ over $B^0 \rightarrow \bar{D}^0K^{*0}$.

We thank the KEKB group for excellent operation of the accelerator; the KEK cryogenics group for effi-

cient solenoid operations; and the KEK computer group, the NII, and PNNL/EMSL for valuable computing and SINET4 network support. We acknowledge support from MEXT, JSPS and Nagoya's TLPRC (Japan); ARC and DIISR (Australia); NSFC (China); MSMT (Czechia); DST (India); INFN (Italy); MEST, NRF, GSDC of KISTI, and WCU (Korea); MNiSW (Poland); MES and RFAAE (Russia); ARRS (Slovenia); SNSF (Switzerland); NSC and MOE (Taiwan); and DOE and NSF (USA).

-
- [1] N. Cabibbo, Phys. Rev. Lett. **10**, 531 (1963); M. Kobayashi and T. Maskawa, Prog. Theor. Phys. **49**, 652 (1973).
- [2] The other unitarity-triangle angles are defined as $\phi_1 \equiv \arg(-V_{cd}V_{cb}^*/V_{td}V_{tb}^*)$ and $\phi_2 \equiv \arg(-V_{td}V_{tb}^*/V_{ud}V_{ub}^*)$.
- [3] L. Wolfenstein, Phys. Rev. Lett. **51**, 1945 (1983).
- [4] K. Abe *et al.* (Belle Collab.), Phys. Rev. Lett. **90**, 131803 (2003).
- [5] T. Aaltonen *et al.* (CDF Collab.), Phys. Rev. D **81**, 031105 (2010).
- [6] A. Poluektov *et al.* (Belle Collab.), Phys. Rev. D **81**, 112002 (2010).
- [7] P. del Amo Sanchez *et al.* (BaBar Collab.), Phys. Rev. D **82**, 072004 (2010).
- [8] P. del Amo Sanchez *et al.* (BaBar Collab.), Phys. Rev. D **82**, 072006 (2010).
- [9] P. del Amo Sanchez *et al.* (BaBar Collab.), Phys. Rev. Lett. **105**, 121801 (2010).
- [10] T. Aaltonen *et al.* (CDF Collab.), Phys. Rev. D **84**, 091504 (2011).
- [11] Y. Horii *et al.* (Belle Collab.), Phys. Rev. Lett. **106**, 231803 (2011).
- [12] R. Aaij *et al.* (LHCb Collab.), arXiv:1203.3662 (2012).
- [13] The charge-conjugate modes are implicitly included unless otherwise stated.
- [14] D. Atwood, I. Dunietz, and A. Soni, Phys. Rev. Lett. **78**, 3257 (1997); Phys. Rev. D **63**, 036005 (2001).
- [15] M. Gronau, Phys. Lett. B **557**, 198 (2003).
- [16] HFAG, online update for Charm at <http://www.slac.stanford.edu/xorg/hfag/charm>.
- [17] B. Aubert *et al.* (BaBar Collab.), Phys. Rev. D **79**, 072003(2009).
- [18] S. Kurokawa and E. Kikutani, Nucl. Instr. and Meth. A **499**, 1 (2003), and other papers included in this volume.
- [19] A. Abashian *et al.* (Belle Collab.), Nucl. Instr. and Meth. A **479**, 117 (2002).
- [20] The Fox-Wolfram moments were introduced in G. C. Fox and S. Wolfram, Phys. Rev. Lett. **41**, 1581 (1978). The Fisher discriminant used by Belle, based on modified Fox-Wolfram moments (SFW), is described in K. Abe *et al.* (Belle Collab.), Phys. Rev. Lett. **87**, 101801 (2001) and K. Abe *et al.* (Belle Collab.), Phys. Lett. **B 511**, 151 (2001).
- [21] H. Kakuno *et al.*, Nucl. Instr. and Meth. A **533**, 516 (2004).
- [22] M. Feindt and U. Kerzel, Nucl. Instr. and Meth. A **559**, 190 (2006).
- [23] K. Nakamura *et al.* (Particle Data Group), J. Phys. G **37**, 075021 (2010) and 2011 partial update for the 2012 edition at <http://pdg.lbl.gov>.